Laboratory course

Terahertz spectroscopy on carrier relaxation in silicon

Instruction manual

Prof. Dr. Roland Kersting
Ludwig-Maximilians-Universität München
LS für Photonik und Optoelektronik

Version: April 17, 2012

Contents

Abstract: Time-resolved terahertz spectroscopy is a novel tool for investigating charge carrier transport in semiconductors. The goal of this experiment is to deduce the charge carriers' momentum relaxation time τ_m in silicon. In the experiment, THz radiation will be time-resolved after transmission through the semiconductor sample. The transmission signal depends on the charge carrier density within the sample, which can be controlled by applying an electrical field. The analysis of differential transmission spectra allows for deducing τ_m with high precision.

1 Goals

Technical goal: Measure the momentum relaxation time of holes in p-doped silicon

Educational objectives: The experiment will introduce to the fundamentals of

1. semiconductor physics: band structure, electrons and holes,
2. carrier transport: Drude model, momentum relaxation, AC conductivity, and
3. experimental techniques: THz technology, modulation spectroscopy, Fourier transforms.

2 Background

2.1 Semiconductors

Recommended literature:

- Hunklinger [1], chapter 10
- Kittel [2], chapter 8
- Ibach, Lüth [3], chapter 12

2.1.1 Fundamental properties of crystals

Inorganic semiconductors such as silicon (Si), germanium (Ge), or gallium arsenide (GaAs) are crystalline. The most common semiconductor crystal structures are the diamond structure (Si & Ge) and the zincblende structure (e.g. GaAs). The conventional unit cells are shown in Fig. 1.

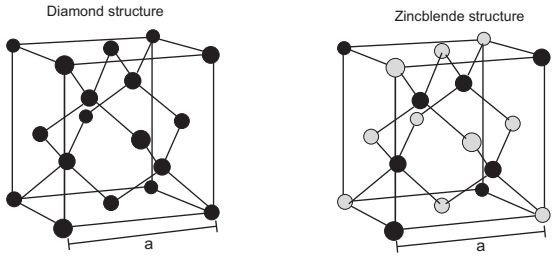

Figure 1: Diamond structure and zincblende structure. Note the different atoms in the zincblende structure. Both structures have lattice constant a.

For understanding the electronic properties of crystals, several models have been developed. They all base of the fact that the crystal lattice is periodic, e.g. with lattice constant a. The Sommerfeld model treats the quantum mechanical properties of electrons as plane waves

$$\psi(\boldsymbol{r}) = const \cdot e^{i\boldsymbol{k}\cdot\boldsymbol{r}} \qquad \text{with energy} \qquad E = \frac{\hbar^2 \boldsymbol{k}^2}{2m} \tag{1}$$

where the wavevector $\boldsymbol{k}$ is quantized

$$k_x = \frac{2\pi n_x}{L} \quad \text{and} \quad k_y = \frac{2\pi n_y}{L} \quad \text{and} \quad k_z = \frac{2\pi n_z}{L} \quad \text{with integer } n_i \text{ and crystal size } L. \tag{2}$$

Figure 2 shows that the dispersion $E(k)$ of the electrons is no longer continuous but has become discrete.

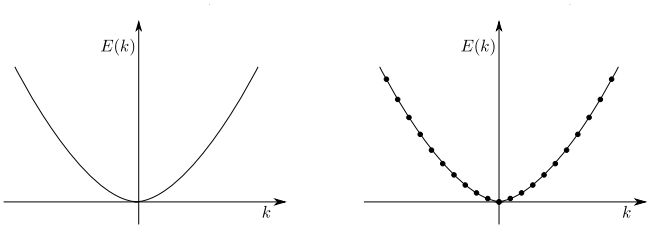

Figure 2: Left: Dispersion of free electrons. Right dispersion of crystal electrons in a one-dimensional (1D) lattice. This hypothetical crystal consists of 20 unit cells, only.

More advanced is the Bloch model, which considers the translational periodicity of electronic waves

$$\psi(r+R) = e^{ikR}\psi(r) \qquad \text{with interatomic distance } R\ . \tag{3}$$

The main result is: In reciprocal space, the dispersion $E(\boldsymbol{k})$ is periodic

$$E(\boldsymbol{k}) = E(\boldsymbol{k}+\boldsymbol{G}) \tag{4}$$

with reciprocal lattice vector $\boldsymbol{G} = \frac{2\pi}{a}$ as shown in Fig. 3. It is sufficient to discuss the band properties in an interval $k\ \epsilon\ \left[\frac{-\pi}{a}, \frac{\pi}{a}\right]$. This is the so called 1st Brillouin zone, or simply the Brillouin zone.

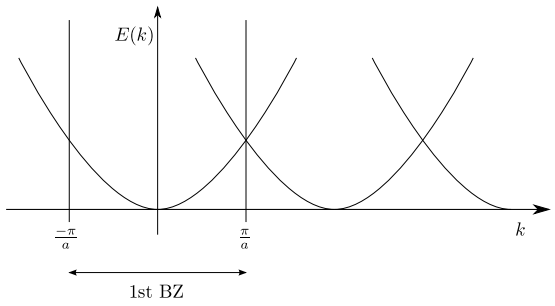

Figure 3: Bloch model of a one-dimensional crystal. The dispersions are periodic with reciprocal lattice vector $G = \frac{2\pi}{a}$.

A further step includes the interaction of the electrons with the binding potential of the atoms. In the most simple approach this periodic potential is weak and of the form

$$V(r) = V_G\ e^{iGr} \quad . \tag{5}$$

Such a potential opens a band gap at the edge of the Brillouin zone (see Fig. 4). Another implication is that the electrons respond to an external force with an inertia m^* that differs from the mass of the vacuum electron m_e.

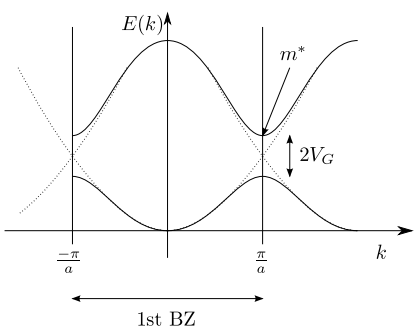

Figure 4: Illustration of the band disperison for a weak potential V_G.

In vacuum, the mass of the electron m_e relates energy E to wavevector k. As can be seen in Fig. 4, the upper band has now a different curvature than the original dispersion of the electron in

vacuum. This is considered by introducing the effective mass:

$$m^* = \frac{1}{\hbar^2}\left[\frac{d^2E}{dk^2}\right]^{-1} \quad . \tag{6}$$

Often the effective mass of the crystal electron differs significantly from the vacuum mass m_e (in case of GaAs $m_e^* = 0.067\ m_e$).

The advantage of the effective-mass concept is that the crystal electrons follow the acceleration theorem

$$\frac{d}{dt}\boldsymbol{k} = \frac{1}{\hbar}\boldsymbol{F} \qquad \text{with force } \boldsymbol{F}\ . \tag{7}$$

This simplifies understanding electronic transport: The crystal electrons can be treated as quasi-particles, [1] which follow the field as described by eq. (7). For transport phenomena, knowledge of the atomic potentials is no longer required. The kinetic response of the crystal electrons can be described by Newton's laws again.

2.1.2 Intrinsic semiconductors

A simplified semiconductor band diagram is shown in Fig. 5. The energy gap E_g separates valence band (VB) and conduction band (CB) and is of the order of 1 eV (see table 1). In case of pure materials, so called intrinsic semiconductors, the Fermi energy E_F is very close to the center of the band gap. At zero temperature, this leads to a valence band filled with electrons and an empty conduction band.

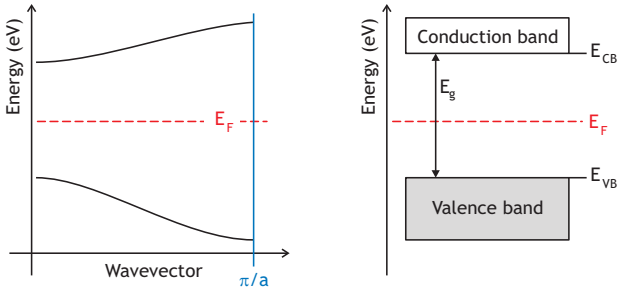

Figure 5: Valence band and conduction band of a semiconductor.

Group IV	$E_g(eV)$	III-V	$E_g(eV)$	II-VI	$E_g(eV)$	I-VII	$E_g(eV)$
diamond	5.48	GaAs	1.42	ZnO	3.20	CuCl	3.39
Si	1.110	InP	1.35	ZnS	3.56	CuBr	3.07
Ge	0.664	InAs	0.36	CdS	2.5	AgF	2.8
SiC	2.42	InSb	0.18	CdTe	1.43		

Table 1: Band gaps of some semiconductors. Most values from Ref. [4].

Even at room temperature $k_BT \ll E_g$ holds and the CB is populated at very low density, due to the fast decay of the Fermi distribution. The remaining empty states in the VB are called holes. They have the same density $n_e = n_h$ since every excited electron leaves a hole behind.

[1] Quasiparticles can be described by energy and wavevector (instead of momentum). When scattering, energy conservation and conservation of wavevector are obeyed. The particle number is not necessarily conserved. Other quasiparticles are: holes, phonons, magnons, plasmons, polarons, and polaritons.

As long as the crystal is in equilibrium, the law of mass action regulates the charge carrier densities in both bands:

$$n_e \cdot n_h = const \tag{8}$$

This holds for intrinsic semiconductors as well as for doped semiconductors. In case of GaAs or Si the intrinsic density ($n_i = n_e = n_h$) is of the order of 10^7 cm^{-3} and 10^{11} cm^{-3}, respectively.

2.1.3 Doped semiconductors

The intention behind doping of semiconductors is to increase the density of one kind of carrier by orders of magnitude. The law of mass action, eq. (8), shows that the density of the other kind of charge carriers is reduced by the same factor.

A semiconductor can be doped by incorporating extrinsic atoms into the semiconductor lattice. For example, Si can be n-doped by arsenic, since only four of the five valence electrons of arsenic can be bound by adjacent Si atoms, leaving one unbound or mobile electron behind.

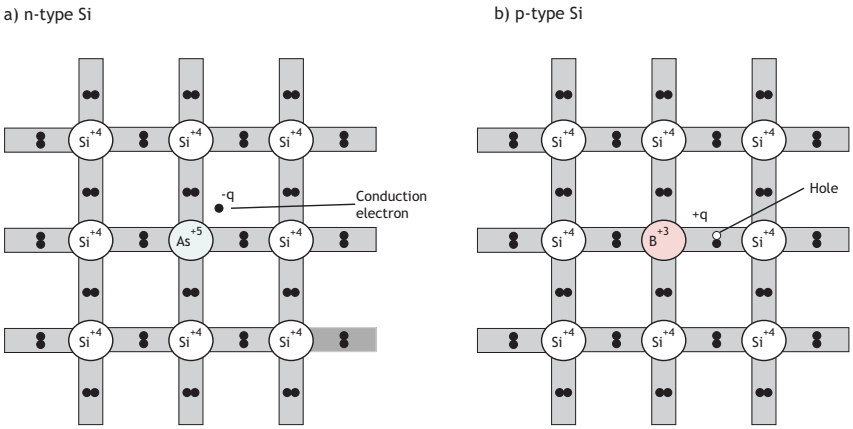

Figure 6: Two-dimensional illustration of saturated bonds in silicon and doping. a) n-type doping by arsenic and b) p-type doping by boron.

In case of n-doping, the dopand atoms are called donors, because they donate a mobile electron to the CB. In case of p-doping the atoms are called acceptors, since they can bind an electron, or using the "hole picture", these atoms donate a hole. One never should forget the remaining ions: They are charged and immobile. Thus, a displacement of the mobile charge carriers leads to the build-up of a Coulomb potential with enormous field strength.

Typical doping densities are in the range 10^{15} cm^{-3} to 10^{19} cm^{-3}, which exceeds the intrinsic density n_i by orders of magnitude. According to the law of mass action, for an n-doped semiconductor $n_e \gg n_h$ holds and for a p-doped semiconductor $n_e \ll n_h$. One consequence is that the Fermi energy has shifted away from the center position within the band gap as illustrated in Fig. 7.

2.1.4 Junctions

The most fundamental semiconductor devices can be achieved by merging n-doped and p-doped materials. Examples are the pn-junction or pn-diode, the pnp-transistor, and the npn-transistor.

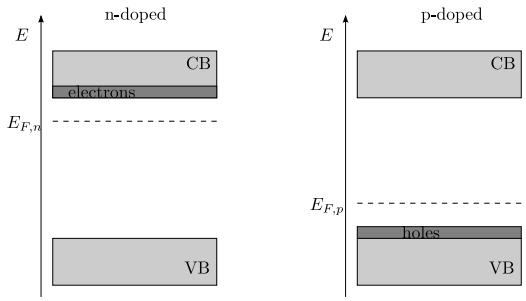

Figure 7: Examples for the position of the Fermi energy in an n-doped semiconductor and in a p-doped semiconductor. For each case only the majority carriers are illustrated.

Another option is to combine a metal with a doped semiconductor, also called Schottky diode. Figure 8 illustrates bands and Fermi energies of a metal and of an n-doped semiconductor.

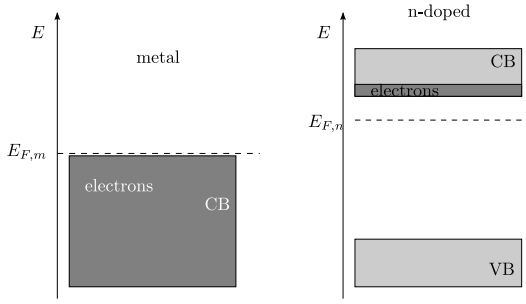

Figure 8: Schematic band diagrams of a metal and of an n-doped semiconductor. Note the difference in Fermi energies.

The metal and the n-doped semiconductor shown in Fig. 8 have different Fermi energies $E_{F,m} \neq E_{F,n}$. This difference leads to the transfer of electrons from the semiconductor into the metal. As soon as the materials are connected, electrons diffuse from the semiconductor towards the metal. One has to remember the immobile donor ions in the semiconductor: Their charge is no longer compensated after electrons got lost to the metal. In consequence, the donor ions cause a Coulomb potential, which warps the band structure as illustrated in Fig. 9.

Now, two important properties can be found: i) the Fermi levels are equilibrated $E_{F,m} = E_{F,n}$ and ii) the semiconductor is depleted from electrons close the junction. The width W of the depletion zone can be calculated from Poisson's equation and is:

$$W = \sqrt{\frac{2\epsilon_0\epsilon_s}{eN_D} \cdot V_{bi}} \tag{9}$$

where ϵ_s is the permittivity of the semiconductor and N_D is the doping concentration. The built-in voltage is $V_{bi} = E_{F,m} - E_{F,n}$.

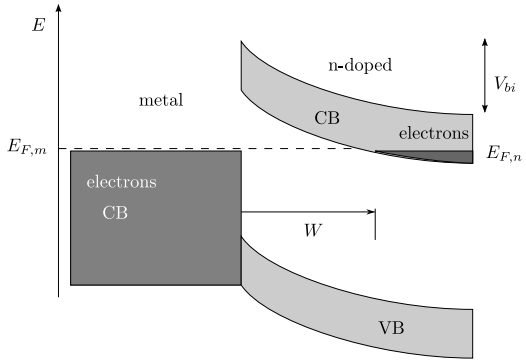

Figure 9: Band structure of a junction between a metal and an n-doped semiconductor. The depletion zone of width (W) is depleted from mobile carriers and behaves as if it were an insulator.

Figure 9 illustrates the equilibrium between metal and semiconductor. Much more interesting is the application of an external voltage V_{ext}. The voltage separates the Fermi energies according

to $eV_{ext} = E_{F,m} - E_{F,n}$. Now the junction is no longer in equilibrium and currents will flow. Additionally, the depletion width changes:

$$W = \sqrt{\frac{2\epsilon_0\epsilon_s}{eN_D} \cdot (V_{bi} - V_{ext})} \tag{10}$$

Thus, the application of a bias controls the width of the depletion zone and the number of mobile charge carriers in the semiconductor. Later we will see that THz radiation interacts with mobile charge carriers. In the experiment, we will use this effect for controlling the strength of the interaction just by the application of the bias.

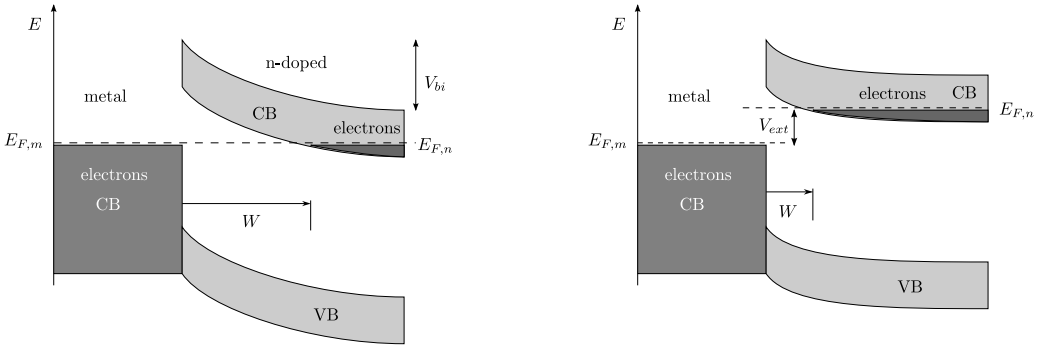

Figure 10: Band structure of a metal semiconductor junction in equilibrium and with an applied bias V_{ext}.

2.2 Carrier transport

Recommended literature:

- Hunklinger [1], chapter 9
- Ibach, Lüth [3], chapter 9
- Ashcroft, Mermin [5], chapter 1

2.2.1 Drude model

One of the first models on charge carrier transport was set up by Paul Drude in 1905 [6]. Mobile charge carriers are assumed to behave as a dilute gas. They respond to external forces and undergo scattering. Between collisions the carriers follow Newton's laws, for instance, when they are accelerated by an electrical field $\mathcal{E}$. The collisions are assumed to be instantaneous and happen at rate $\gamma = \frac{1}{\tau_m}$ where τ_m is the average time interval between scattering events, or in other words, the time of momentum relaxation.

2.2.2 DC conductivity

The conductivity σ relates the current density j to the driving electric field $\mathcal{E}$ in the material:

$$j = \sigma\, \mathcal{E} \tag{11}$$

If the conductor has cross section A and v is the electron velocity perpendicular to A, then the number of electrons, which cross A in a unit time dt is $n\ v\ A\ dt$ and the resulting flow of charge is $-e\ n\ v\ A\ dt$. The current density is then given by:

$$j = \left.\frac{I}{A}\right|_{\perp} = \frac{-e\ n_e\ v\ A\ dt}{A\ dt} = -n_e\ e\ v \quad . \tag{12}$$

After a collision, an electron gains velocity in the field

$$v(t) = \frac{-e\mathcal{E}}{m} t \tag{13}$$

where t is the time after the last collision. For the average velocity of the charge carriers we get:

$$v_{avg} = \frac{-e\mathcal{E}}{m^*}\tau_m \tag{14}$$

where we already used the effective mass m^* since we have to consider crystal electrons. With eq. (12) we get the current density

$$j = \frac{n_e e^2 \tau_m}{m^*}\mathcal{E} \qquad \text{and} \qquad \sigma_{DC} = \frac{n_e e^2 \tau_m}{m^*} \quad . \tag{15}$$

This direct current conductivity σ_{DC} describes the response to a constant field $\mathcal{E} = const.$

2.2.3 AC conductivity

This section deals with the charge carriers' response to a time-dependent field $\mathcal{E}(t)$. The classical momentum of an electron can be described by [2]

$$\frac{d}{dt}p + \frac{1}{\tau_m}p = -e\mathcal{E}(t) \quad . \tag{16}$$

We use the ansatz:

$$p = p(\omega)\cdot e^{+i\omega t} \qquad \text{and} \qquad \mathcal{E}(t) = \mathcal{E}_0(\omega)\cdot e^{+i\omega t} \tag{17}$$

and get

$$i\omega\cdot p(\omega) + \frac{1}{\tau_m}p(\omega) = -e\cdot\mathcal{E}_0(\omega) \quad \Rightarrow \quad p(\omega)\left[\frac{1}{\tau_m} + i\omega\right] = -e\cdot\mathcal{E}_0(\omega) \quad . \tag{18}$$

In this case electrons cause a complex-valued current density $\tilde{j} = -n_e e p/m^*$ or:

$$\tilde{j}(\omega) = \frac{n_e e^2}{m^*}\cdot\frac{\tau_m}{1+i\omega\tau_m}\cdot\mathcal{E}_0(\omega) \quad . \tag{19}$$

This provides the conductivity for alternate currents, the AC conductivity:

$$\tilde{\sigma}_{AC} = \frac{n_e e^2}{m^*}\cdot\frac{\tau_m}{1+i\omega\tau} \quad , \tag{20}$$

[2] We use here the classical velocity and the classical momentum, which is in accord with Drude's ansatz of a gas. For a quantum mechanical treatment it is more appropriate to discuss the change of wavevector k. The results, however, are identical.

which depends on frequency ω and can be expressed using the DC conductivity as

$$\tilde{\sigma}_{AC} = \sigma_{DC} \cdot \frac{1}{1 + i\omega\tau_m} = \sigma_{DC} \cdot \frac{1 - i\omega\tau_m}{1 + \omega^2\tau_m^2} \quad . \tag{21}$$

2.3 Terahertz technology

In solid state, typical momentum relaxation rates are of the order of 100 fs $= 10^{-13}$ s. Experiments that resolve the electronic motion in time-domain therefore require ultrafast time-resolution. This is provided by THz technology, which was developed over the past twenty years. The so called THz range extends from frequencies of about 100 GHz to about 10 THz. The corresponding wavelengths are 3 mm and 30 μm.

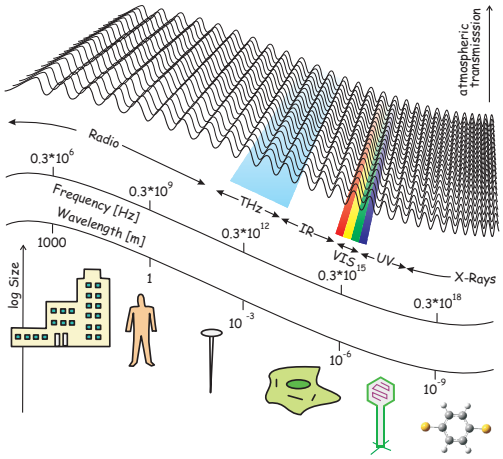

Figure 11: Illustration of the accessible electromagnetic spectrum, the atmospheric transmission and relation of the wavelength to comparable objects.

Time-resolved THz spectroscopy utilizes coherent pulses of electromagnetic radiation as shown in Fig. 12. Terahertz spectroscopy differs from spectroscopy in the visible range by the fact that the electric field is measured and not the time-averaged light intensity. One important consequence is that amplitude and phase can be obtained in a single measurement. It can be shown that this allows for measuring the real part of $\tilde{\sigma}_{AC}$, as well as its imaginary part.

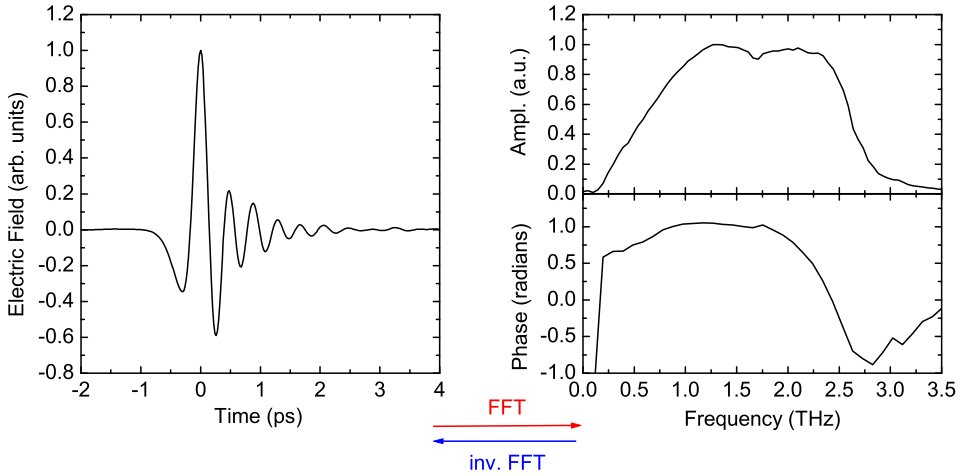

Figure 12: Terahertz pulse and corresponding spectra of amplitude and phase. The spectra of amplitude and phase can be obtained by numerical fast-Fourier transformation.

2.3.1 Generation of THz pulses

First of all, THz measurements require the generation of THz pulses. This is usually achieved by illuminating semiconductor structures with ultrafast laser pulses. The photoabsorption leads to the generation of electrons and holes in the semiconductor. As soon as the charge carriers are generated, they are accelerated in the electric field applied by the metal contacts on top of the structure. According to Maxwell's equations the acceleration leads to the emission of radiation (Bremsstrahlung). The superposition of the emissions constitutes the THz pulse.

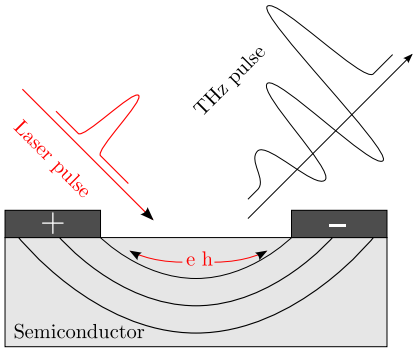

Figure 13: Illustration of the generation of THz radiation in a GaAs structure. An ultrafast laser pulse generates electrons and holes in the semiconductor structure. The charge carriers are accelerated by the applied field and emit coherent THz radiation.

2.3.2 Time-resolved detection of THz pulses

The oscillation of THz pulses is too fast for a direct detection by electronic means. Such ultrafast time-resolutions become accessible by correlation techniques. In our case, we record the cross-correlation between the THz pulse and a laser pulse:

$$\mathcal{C}(t_{opt}) = \lim_{T\to\infty} \frac{1}{T} \int_{-T/2}^{T/2} \mathcal{E}_{THz}(t') \cdot \mathcal{I}_{laser}(t' + t_{opt})\ dt' \tag{22}$$

with time-delay t_{opt} between the THz pulse and an ultrafast laser pulse. Provided that the laser pulse is much shorter than the oscillation time of the THz pulse, we can say that $\mathcal{E}(t) \sim \mathcal{C}(t_{opt})$. The delay of t_{opt} can be easily achieved by controlling the length of optical paths, e.g. by mirrors and motorized translation stages (see Fig. 14). A delay of 100 fs corresponds to a mirror displacement of about 15 μm, given by the speed of light.

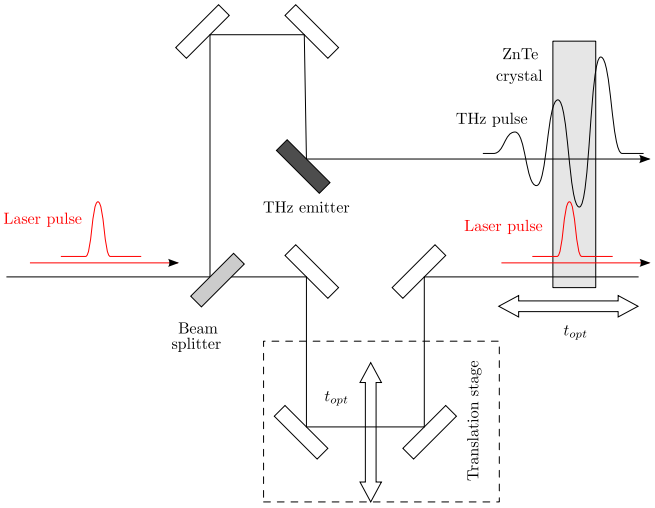

Figure 14: An ultrafast laser pulse is time-delayed by mirror optics and a translation stage. The THz pulse rotates the polarization of the laser pulse within the ZnTe crystal.

The correlation requires an interaction between the THz pulse and the laser pulse. This can be achieved in nonlinear optical crystals. We will use ZnTe and the nonlinear effect is called Kerr-effect. Here, the field of the THz pulse rotates the polarization of the laser pulse as illustrated in Fig. 15. The rotation is proportional to the electric field of the THz pulse. Depending on the time-delay, rotations to the right, as well as to the left occur. With this process the information on the THz pulse is copied onto the light pulse. Finally, the polarization of the laser pulse can be read out by standard polarization optics and two photodiodes, each detecting a different polarization. But the process in the Kerr medium is weak. Typical rotations are of the order of 10^{-4}, which requires advanced electronics for reading out the photodiodes.

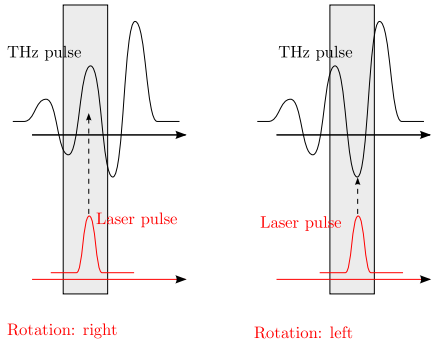

Figure 15: In nonlinear materials such as ZnTe, the THz pulse rotates the polarization of the laser pulse. The direction of rotation depends on the sign of the THz field.

Altogether, recording an entire THz transient requires many measurements, each at a different time-delay between THz pulse and laser pulse. This is achieved by moving the translation stage in micrometer-size steps, which is usually done by a computer control and a measurement program.

3 Experimental

3.1 Setup for THz time-domain spectroscopy

A schematic of the experimental setup is shown in Fig. 16. We use a femtosecond laser source, (Mai Tai of Spectra Physics) which delivers 80 fs pulses at a repetition rate of 80 MHz. The wavelength is about 780 nm and the average output power is approximately 0.8 W. [3] In front of the vacuum chamber, a beam-splitter (not shown in Fig. 16) divides the laser light into two beams. Also not shown is the translation stage for the time-delay, which is located outside the chamber.

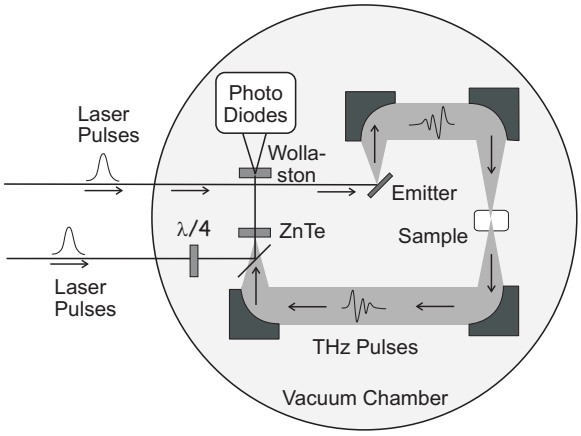

Figure 16: Schematic of the THz setup. Beam splitter as well as the translation stage for the time-delay are outside of the chamber and are not shown here.

3.2 Silicon sample

The center goal of the experiment is the measurement of the charge carriers' momentum relaxation time τ_m in silicon. The sample consists of a silicon chip p-doped at $N_A = 2 * 10^{15}$ cm^{-3}. At room temperature, all acceptors are ionized and $n_h = N_A$. Two ohmic contacts to the hole gas in the silicon are at the side of the sample (see Fig. 17). The top surface is covered by 300 nm SiO_2. On this surface a chromium contact (gate contact) with a thickness of 7 nm has been deposited.

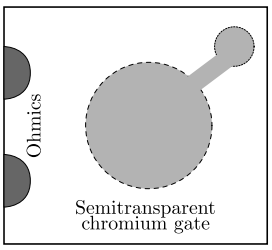

Figure 17: Illustration of the silicon sample. Electrical contact to the holes is made by two ohmic contacts. The semitransparent Cr layer can be understood as a top gate under which the hole density will be modulated. The THz beam will have to impinge in the center of this Cr layer.

Underneath the gate contact, the hole density can be controlled as illustrated in Fig. 18. The application of a positive bias V_{ext} at the gate contact lifts the silicon band structure and the depletion width W increases. This reduces the number of holes along the path of the THz beam. The interaction between THz beam and the holes is proportional to the two-dimensional density $n_{2D} = n_h \cdot \Delta W$. This allows for controlling the interaction by application of V_{ext}.

[3] Even laser powers of 0.001 W may damage the eye. Wearing laser goggles is mandatory during the experiment.

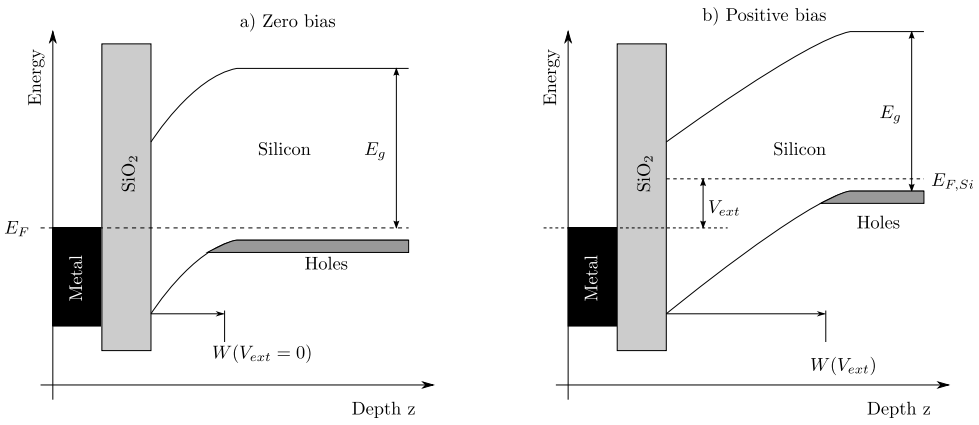

Figure 18: Band diagram of the sample. a) without external bias V_{ext} and b) with $V_{ext} > 0$.

3.3 Modulation spectroscopy

In terahertz modulation spectroscopy, two transients of the electrical field will be recorded:

- the transmitted field $\mathcal{E}_0(t)$, when no bias is applied $V_{ext} = 0$
- the transmitted field $\mathcal{E}_1(t)$, with bias $V_{ext} \neq 0$

The relative difference of the two curves $\Delta\mathcal{E}(t) = \mathcal{E}_1(t) - \mathcal{E}_0(t)$ is just about 1/200 (see Fig. 19).

The difference signal is proportional to the motion of the charge carriers when driven by the field. In rough approximation, the field emitted by the charge carriers is

$$\Delta\mathcal{E}(t) \sim \frac{\partial}{\partial t} j(t) \sim \frac{\partial}{\partial t} v(t) \sim \frac{\partial}{\partial t} \sigma_{AC} \mathcal{E}_0(t) \quad . \tag{23}$$

Using the ansatz $\mathcal{E}_0(t) = \hat{\mathcal{E}}_0 e^{i\omega t}$ will show that the differential THz signal is proportional to the displacement of the charge carriers. The lower curve in Fig. 19 is proportional to the displacement of the holes when driven by the THz field.

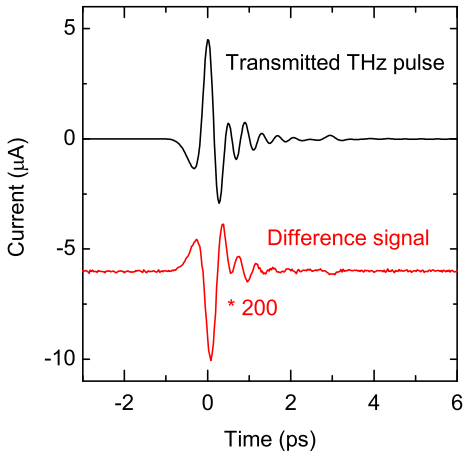

Figure 19: Data obtained on a silicon structure. The upper curve shows the transmitted THz signal $\mathcal{E}_0(t)$. The lower curve is obtained from two measurements one performed without an external bias applied to the silicon structure and one with $V_{ext} = 20$ V. The curve shown is the difference $\Delta\mathcal{E}(t)$. It is proportional to the displacement of the carriers by the THz pulse and thus shows the motion of the carriers.

A more rigorous treatment [7] uses the AC conductivity and yields for the relative change of the transmitted field

$$S = \frac{\Delta\mathcal{E}}{\mathcal{E}_0} \approx -\Delta W \frac{Z_0}{2n_{Si}}\sigma_{AC} \qquad \text{with} \qquad \sigma_{AC} = \frac{n_h e^2 \tau_m}{m_h^*} \cdot \frac{1 - i\omega\tau_m}{1 + \omega^2\tau_m^2} \tag{24}$$

where $n_{Si} \approx 3.5$ is the index of refraction of silicon and $Z_0 = 377\ \Omega$ is the impedance of vacuum.

The above equations suggest the discussion of the measurement signals in frequency-domain. As can be seen from eq. (24) the quantity $S(\omega)$ is complex valued. A useful relationship can be achieved by dividing the imaginary part of S by the real part:

$$\frac{\Im\ S(\omega)}{\Re\ S(\omega)} = -\omega\tau_m =: \tan\phi \tag{25}$$

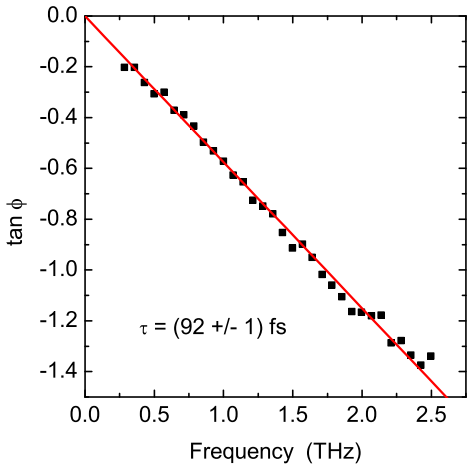

Figure 20: Relation between phase and frequency ν. The dots show data from the transients in Fig. 19. The line is a linear fit.

Thus a plot of $\tan\phi$ versus frequency $\nu = \frac{\omega}{2\pi}$ will exhibit a negative slope, which is just the momentum relaxation time $\tau_m/2\pi$. Figure 20 shows this relation in frequency-domain. The data were obtained by Fourier transform from the time-resolved measurements of Fig. 19. The good agreement between experimental values and fit shows that τ_m can be deduced with high precision.

3.4 Measurement procedure

The signals detected by the photodiodes are orders of magnitude smaller than the background without any THz pulse. The extraction of such tiny signals is usually done with a lock-in amplifier (LIA) and a chopper, which periodically blocks the THz beam. The LIA locks the internal signal amplification to the frequency, at which the laser beam is chopped. This suppresses the background as well as the noise. Instead of using a mechanical chopper, we apply an alternate bias at 63 kHz to the THz emitter (Fig. 13). Fundamentals of LIAs can be found in appendix 5.3.

The computer records the output of the LIA for every time-delay t_{opt} . This procedure would suffice for recording a single transient. In our experiment, however, we have to detect two transients $\mathcal{E}_0(t)$ and $\mathcal{E}_1(t)$. In principle, one could record the curves sequentially. The disadvantage of this procedure is that the laser is noisy, which makes it difficult to see such small differences as the modulation

signal. [4] A significant reduction in noise is achieved when recording the two transients in parallel. For this purpose a square voltage V_{ext} at a frequency of a few thousand Hertz is applied to the silicon structure. For every time-delay the translation stage stops for about one second and the computer records 100,000 samples of the applied voltage as well as of the THz signal delivered by the LIA. The rest is averaging in dependence on high and low thresholds as illustrated in Fig. 21.

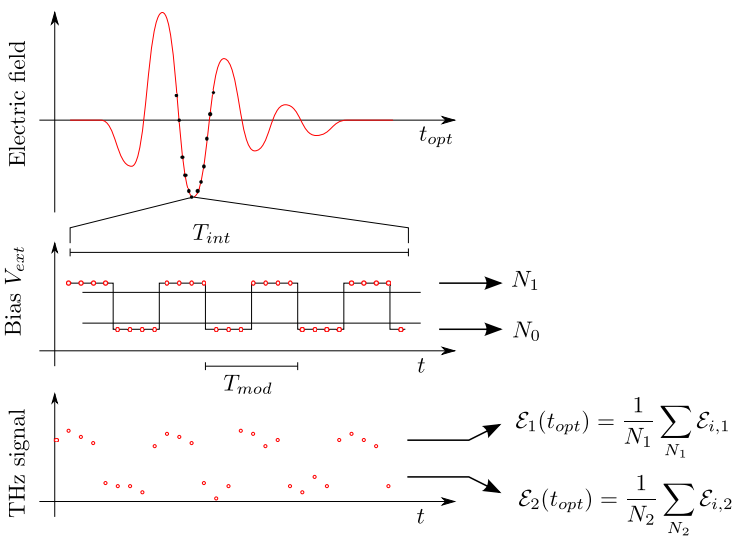

Figure 21: Schematic of transient modulation spectroscopy. The upper curve illustrates a THz transient as it may be transmitted through the sample. For every optical time-delay t_{opt}, the bias at the sample is modulated for an integration time T_{int} at frequency $\nu_{mod} = 1/T_{mod}$. The computer records the applied bias V_{ext} as well as the THz signal $\mathcal{E}_i$. Two thresholds of V_{ext} define whether the corresponding signal $\mathcal{E}_i$ belongs to the record with high bias or to the record with low bias. Finally, the averages are computed.

3.5 Measurement plan

Task 1: Record one THz transient while the chamber is vented and another transient in vacuum. The normalized amplitude spectrum will show many absorption lines. How do you interpret the result?

Task 2: Measure two THz transient in vacuum. One without the Si sample and one with. The signal obtained with the structure will have reduced field and will be shifted in time-domain by about 7 ps. How do you interpret these observations?

Task 3: Measure the momentum relaxation rate of the holes in the Si structure. Apply a square bias between 5 and 15 V at a frequency of about 3323 Hz. Ask the teaching assistant (TA) before you connect the silicon structure to the frequency generator. A wrong bias may blow the structure and a replacement costs the TA a weak of cleanroom work. Use the data evaluation software and extract τ_m.

[4] In rough approximation, all devices introduce noise, which scales with the measurement frequency as $\frac{1}{f}$. It is therefore advantageous to switch rapidly between the two measurements back and forth.

3.6 Data analysis

We will supply you with two programs for data analysis:

- **FFTman:** This is a program for manipulating data sets of complex numbers, which includes fast Fourier transforms (FFTs).
- **ExtractTau:** This program extracts τ_m from $\mathcal{E}_0(t)$ and $\mathcal{E}_1(t)$.

Task 1: Use the program FFTman.

1. Load up the transients you obtained in task 1. For instance, store the transient obtained in air in slot 1 and store the transient obtained in vacuum in slot 2. [5]
2. Do the FFTs of slot 1 and slot 2 and store your results, for instance, in slot 3 and 4.
3. If you plot these slots, you will see an unusable curve. The reason is that your FFT data are in the format frequency, real part and imaginary part.
4. Convert the results stored in slot 3 and 4 into amplitude and phase and store the results, for instance, in slot 6 and 7. Careful, you know that these slots are now amplitude and phase data, but the computer program doesn't. If you continue with manipulating these data sets, the program will handle them as if they would be real and imaginary data.
5. In the end you will have two amplitude spectra, which you may want to discuss.
6. Save the data and make print-outs for your lab report.

Task 2:

1. Use commercial software such as Origin, or public domain software such as GNU-Plot.
2. Plot the two transients recorded with and without sample in a single sheet.
3. Analyze the shift in time-delay, as well as the reduction in field strength.
4. Make print-outs for your lab report.

Task 3:

1. Use program ExtractTau.
2. Load up the data array obtained by modulation spectroscopy. This consists of a the following columns: time-delay, E_0, and E_1.
3. When you start the program, it will automatically:
   - calculate the difference between the two transients $\Delta\mathcal{E}$
   - do the FFTs on $\mathcal{E}_0$ and on $\Delta\mathcal{E}$
   - calculate $\tan\phi = \frac{\Im S(\omega)}{\Re S(\omega)}$
4. Finally, the program will fit a line to the result and will display τ_m and the error $\Delta\tau_m$.
5. Make print-outs for your lab report.

[5] The original data are two column, one for the time-delay and one for the measured field. The program, however, will add a third, which is the imaginary field (it is zero for all time-delays). This procedure gives the program a little bit more flexibility: Now you can do fast Fourier transforms (FFTs) and then the inverse (invFFT) and you will get the original curve again.

4 Outlook: Modern materials

Today, novel electronic materials are developed at enormous rate. Usually, only small quantities are synthesized, for instance, as a thin film deposited on a substrate (Fig. 22). Many new materials may have application potential, but this requires the characterization of electronic transport properties. The electronic characterization of a thin film is challenging. As illustrated in Fig. 22 electronic transport may be hindered by trapping of the charge carrier into a defect (b) or by the transfer across grain boundaries (c). Both processes delay the charge transport from one contact to the other substantially. Additionally, currents through the substrate may spoil conductance measurements. Altogether, these processes make it nearly impossible to conclude on the charge transport of the material itself.

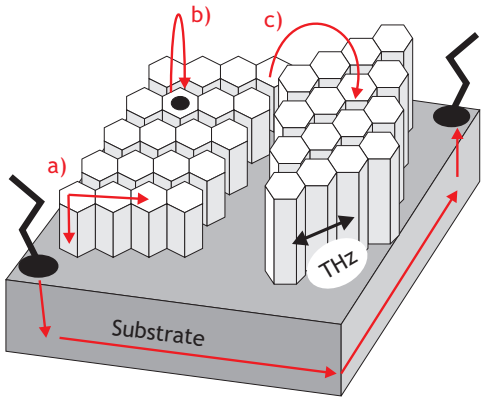

Figure 22: Illustration of a thin film on a substrate.

The advantage of THz experiments is that the charge carrier propagates only fractions of a nanometer when driven by the THz pulse. A good estimate is:

$$\Delta x \approx v_{avg} \cdot T_{osc} = \mu \mathcal{E} T_{osc} \qquad \text{with} \qquad \mu = \frac{e\tau_m}{m^*} \tag{26}$$

where T_{osc} is the oscillation time of the THz field and μ is the mobility of the charge carrier. The THz field is of the order $\mathcal{E} \approx 10,000$ V/m. If we use for μ the hole mobility in silicon ($\mu \approx 200$ cm^2/Vs) we get $\Delta x \approx 2$ Å. Such small displacements make it highly improbable that the charges have to cross a grain boundary. Transport properties obtained by THz spectroscopy come close to those of a future, perfect material. In consequence, THz spectroscopy provides an early view on the potential of a novel material long before perfect films or crystals can be fabricated.

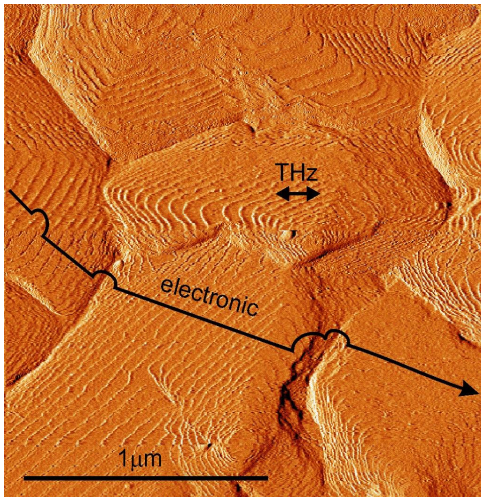

Figure 23: Atomic force micrograph of a pentacene layer. Pentacene is a modern organic semiconductor. The difference between conventional electronic characterization and THz characterization is illustrated, too.

5 Appendix

5.1 Safety instructions

1. Improper use of instrumentation may cause damage or may be even dangerous. It is absolutely necessary that you follow these safety instructions and the instructions of the teaching assistant (TA).
2. Use only the equipment, which was given to you by the TA.
3. Use the equipment only for the purpose it is designed for. In case of concerns or uncertainty, ask the TA.
4. Due to the high laser power, wearing laser goggles is mandatory. Ask the TA for appropriate laser goggles.
5. Do not change or touch the mirror optics on the optical table. Slight misalignments are fatal!
6. Do not change electrical wiring or voltages of the devices unless instructed by the TA.

We understand that you are familiar with these safety instructions and that you accept them.

5.2 Electrical circuitry

The electrical circuitry is schematically illustrated in Fig. 24. The current delivered by the photodiodes is proportional to the intensity difference between the two polarizations of the laser beam. This signal is amplified by a transimpedance preamplifier (SR570). The output voltage is fed to the lock-in amplifier (LIA, SR860). The LIA provides a high frequency sine voltage for modulating the THz emitter, too. The signal output of the LIA is digitized by an analog-digital (AD) converter.

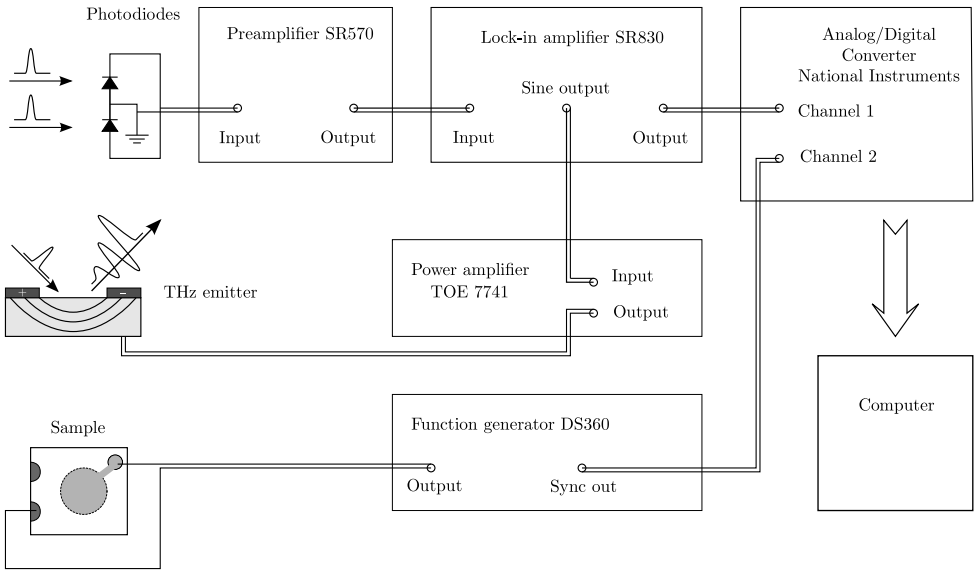

Figure 24: Schematic of the electric circuitry. All connections are made with BNC (Bayonet Neill–Concelman connectors) cables.

The sample is modulated by a square voltage V_{ext} provided by a function generator (DS360). The synchronized output is proportional to V_{ext} and is digitized by the AD converter, too. These signals are delivered to the computer. The measurement program records the data and also controls the position of the optical time-delay (not shown in Fig. 24).

5.2.1 Settings of the preamplifier SR570

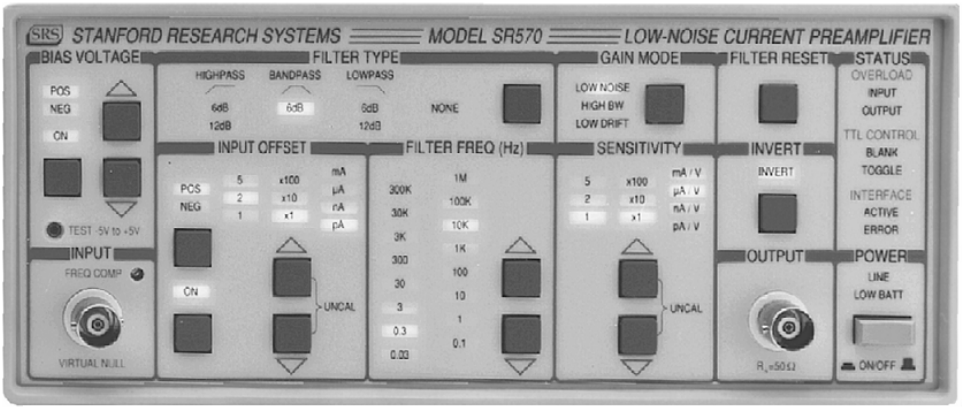

Figure 25: Current pre-amplifier SR570. Picture from manuals of SRS: http://www.thinksrs.com/.

Caution:

- There is no need adjusting the settings of the SR570. The TA will have done this for you.
- In case you want to change the settings: Call the TA. He will supervise your work.

Bias voltage: off

Filter type: none

Input offset: off

Filter frequency: (not active)

Gain mode: low noise

Sensitivity: 1 mA/V

Invert: on/off depending on the THz-transient this can mirror the transient about the time-axis compensating for a wrong polarization of the laser pulse

5.2.2 Settings of the LIA SR830

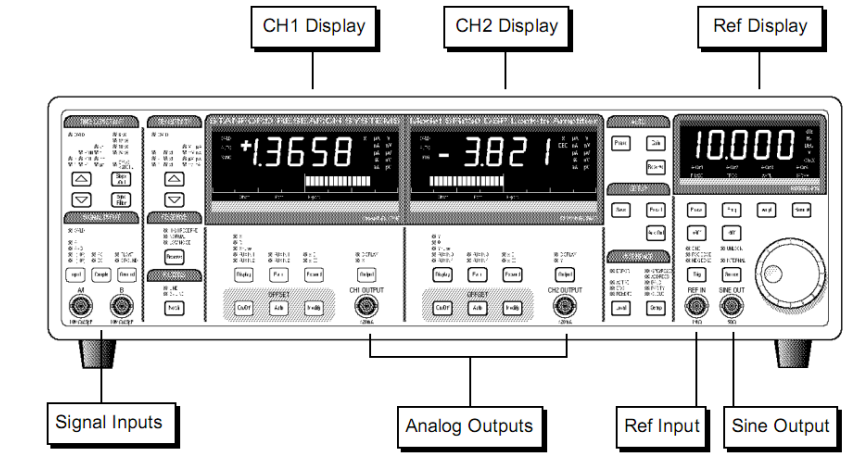

Figure 26: Lock-in amplifier SR830. Picture from manuals of SRS: http://www.thinksrs.com/ .

Caution:

- There is no need adjusting the settings of the LIA. The TA will have done this for you.
- Wrong settings may cause damage of instrument and sample. We strongly recommend not changing the parameters!
- In case you want to change the settings: Call the TA. He will supervise your work.
- Careful: the amplitude of the internal oscillator should not exceed 0.6 V. This voltage is fed to the power amplifier and drives the THz emitter. If the voltage exceeds 0.6 V, the THz emitter may be damaged.
- In case you observe a wrong setting, ask the TA.

Time constant:

- 10 μs for 102.4 kHz sampling with the AD-card,
- 100 ms/10 ms for direct scan with LIA.

Sensitivity: 20 mV , **Slope:** 24 dB/oct , **Sync Filter:** off

Signal Input: A, **Coupling:** AC, **Ground:** Ground

Reserve: Low Noise, **Filters:** Off

Channel 1: Display: X, Output: X , Output connected to channel 1 of AD-card

Channel 1: Ratio, Expand and Offset: Off

Channel 2: Display: Y, Output: Y

Channel 2: Ratio, Expand and Offset: Off

Trigger: Sine , **Source:** Internal, **Harmonic:** 1

Frequency: We suggest 63.17 kHz.

Amplitude: 0.6 V. Do not use higher voltages. This may damage the THz emitter.

5.2.3 Settings of the function generator DS360

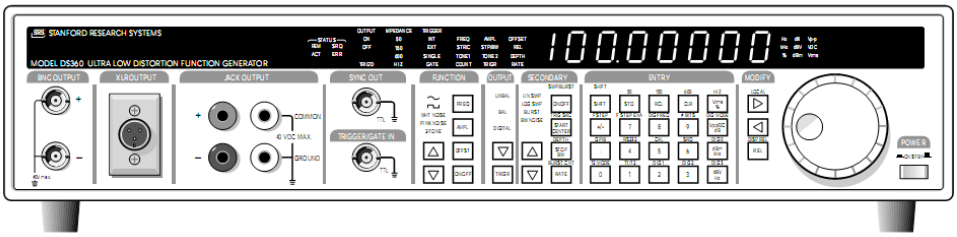

Figure 27: Function generator DS360. Picture from manuals of SRS: http://www.thinksrs.com/.

Caution:

- There is no need adjusting the settings of the DS360. The TA will have done this for you.
- Wrong settings may cause damage of instrument and sample. We strongly recommend not changing the parameters!
- In case you observe a wrong setting, ask the TA.

Output: Connect OUTPUT BNC to the oscilloscope's CH1. If all values are ok (see section 5.2.5) then connect to the sample.

Sync out: Connect SYNC OUT to CH2 of the oscilloscope . If all values are ok (see section 5.2.5) then connect to Channel 2 of the AD-card.

Offset: $(V_{ext}^{max} + V_{ext}^{min})/2$, Volt DC, for instance 15 V

Amplitude: $V_{ext}^{max} - V_{ext}^{min}$, Volt Vpp AC, for instance 10 V

Function: Rectangular

Frequency: Something between 5 Hz and 5 kHz. We suggest 3323 Hz.

Mode: Unbalanced

Modify function: SWP/BURST: off

In case you want to change settings proceed the following way:

1. Switch the output off.
2. Disconnect sample and AD card.
3. Connect to CH1 and CH2 of the scope.
4. Switch output to on.
5. Check your signal on the scope and change settings of the function generator if necessary.
6. If everything is alright: Connect to the sample again.

5.2.4 Settings of the amplifier TOE 7741

Figure 28: High-power amplifier TOE 7741. Picture from manuals of Toellner.

Caution:

- There is no need adjusting the settings. of the TOE7741.
- Wrong settings may cause damage of the THz emitter. We strongly recommend not changing the parameters!
- In case you observe a wrong setting, ask the TA.

5.2.5 Settings of the oscilloscope Voltcraft 630-2

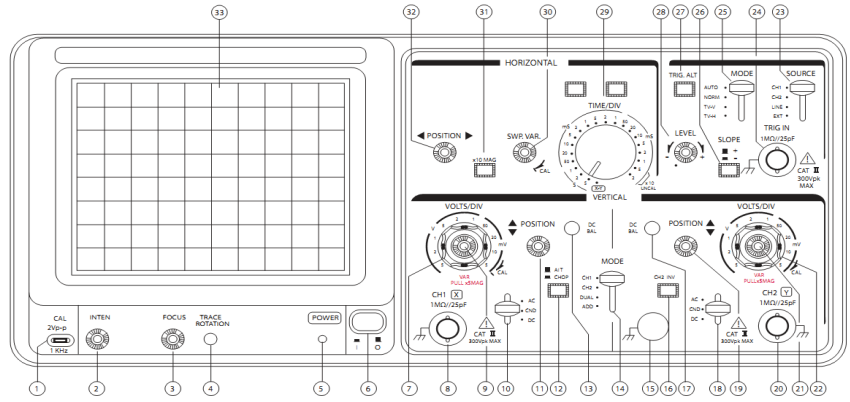

Figure 29: Oscilloscope. Picture from manual of Voltcraft 630-2.

Use the scope for checking the output of the function generator.

1. Make sure the output of the function generator is switched off.
2. Disconnect the sample from the function generator.
3. Connect the output (BNC OUTPUT +) of the function generator, as well as the SYNC OUT signal to CH1 and CH2 of the scope, respectively.
4. Set the trigger to CH2.
5. When properly adjusted, you should see two square signals on the scope.
6. Read off the amplitudes and compare them to the desired values. These are $V_{ext} \epsilon [5 - 15]$ V and $V_{sync} \epsilon [0 - 5]$ V.
7. If this is the case, and only then, you may connect the sample.

5.3 Background: Lock-in amplifiers

In research, measurement signals are often very weak and infested by noise. Additionally, an unwanted background signal may exceed the original signal by orders of magnitude. Lock-in amplifiers (LIAs) are the standard tool for extracting the signal and for reducing noise.

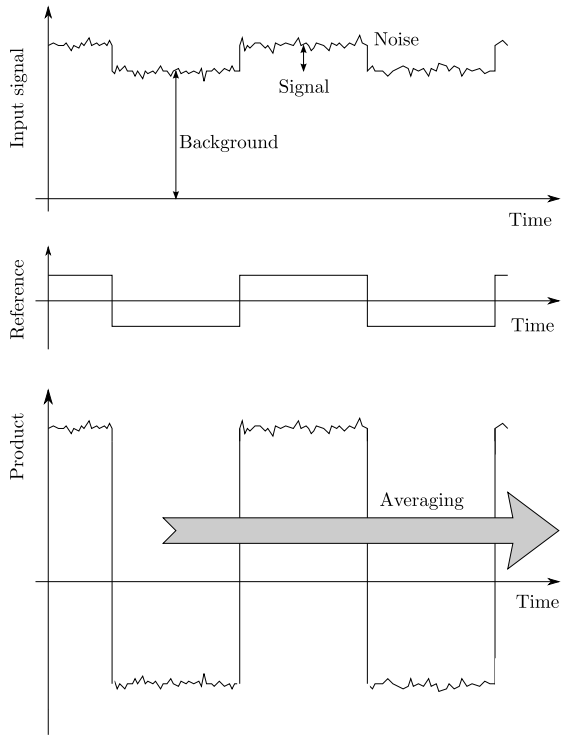

Figure 30: Signal processing with a LIA. Upper curve: Input signal of the LIA. The chopper switches the signal to be measured on and off. The background signal may be much stronger than the targeted signal. Middle curve: Reference signal, which is in phase with the chopper. Lower curve: The product of the upper curves.

Figure 30 illustrates the signal processing within a LIA. The signal is much smaller than the background and may be even smaller than the noise. Chopping the original signal leads to a time-dependent input as illustrated by the upper curve. Usually, the order of the time scale is μs to ms (in our experiment we use a frequency of about 63 kHz). The reference signal coming from the chopper will be in phase with the input signal of the LIA. The mixer of the LIA multiplies input signal and reference. The resulting product is shown by the lower curve.

The output signal of the LIA is the time average of the product. In modern digital LIAs this is done by numerical integrating algorithms. Together, mixing and averaging rejects noise at all those frequencies, which differ from the reference frequency. Obviously, the averaging time should be at least one modulation period.

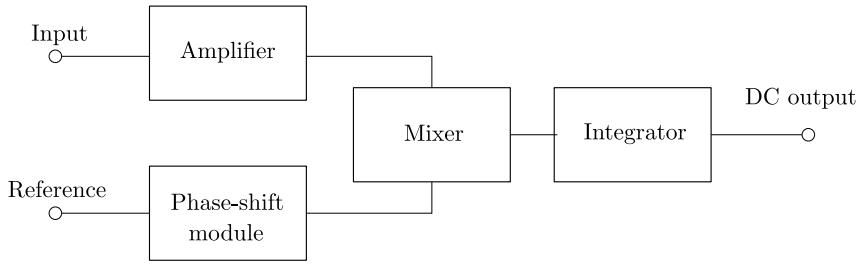

Figure 31: Simplified block diagram of a lock-in amplifier.

References

[1] S. Hunklinger, *Festkörperphysik* (Oldenbourg, 2007).

[2] C. Kittel, *Introduction to Solid State Physics* (John Wiley and Sons, 2002).

[3] H. Ibach, H. Lüth, *Festkörperphysik* (Springer, 2000).

[4] J. Solyom, *Fundamentals of the Physics of Solids*, vol. 2 (Springer, 2007).

[5] N. Ashcroft, N. Mermin, *Solid State Physics* (Holt, Rinehart and Winston, 1987).

[6] P. Drude, *Ann. d. Physik* **1**, 566 (1900).

[7] S. Funk, G. Acuna, M. Handloser, R. Kersting, *Opt. Expr.* **17**, 17450 (2009).